SABA Publishing

Journal of Fractional Calculus and Nonlinear Systems
jfcns.sabapub.com
ISSN : 2709-9547

J Frac Calc & Nonlinear Sys
(2026)7(1) : 73-102
doi:10.48185/jfcns.v7i1.2064

NUMERICAL SIMULATIONS AND CONTROL STRATEGIES FOR COVID-19 AND MONKEYPOX CO-INFECTION DYNAMICS

FRANKLINE C. EZE [a,*], MARTIN C. OBI[b], ANTHONY I. NWADIBIA. [c], KELVIN N.C. NJOKU [d], DOMINIC I. ALFRED [e]

[a] Department of Mathematics and Statistics, Federal Polytechnic Nekede, Owerri, Nigeria
[b] Department of Mathematics, Federal University of Technology, Owerri, Nigeria
[c] Department of Mathematics and Statistics, Federal Polytechnic Nekede, Owerri, Nigeria
[d] Department of Mathematics, Imo State University, Owerri, Nigeria
[e] Department of Mathematics and Statistics, Federal Polytechnic Nekede, Owerri, Nigeria

• *Received: 21 April 2026* • *Accepted: 09 June 2026* • *Published Online: 30 June 2026*

Abstract

This study is a continuation of [16], which developed a deterministic model for the co-infection dynamics of COVID-19 and Monkeypox, including model formulation, basic properties, reproduction numbers, and stability analyses of both disease-free and endemic equilibria. In this extension, we further investigate key dynamical aspects of the system that were not previously addressed. Specifically, we establish the existence and uniqueness of solutions using the fixed point theorem, perform sensitivity analysis of the basic reproduction numbers for both diseases to identify key epidemiological parameters driving disease transmission, and formulate an optimal control problem to determine effective intervention strategies. Furthermore, numerical simulations are carried out using Python to illustrate the theoretical results and to provide insight into the impact of control measures on disease dynamics. The results obtained provide deeper understanding of the model behavior and offer useful guidance for designing efficient strategies to mitigate the co-infection burden of COVID-19 and Monkeypox.

Keywords: COVID-19; Monkeypox; Co-infection dynamics; Vaccination; Numerical simulation; Sensitivity Analysis.

1. Introduction

Infectious diseases continue to be one of the most critical challenges to the health of the population globally [20], especially under conditions that promote increased human mobility, urbanization, climate change, and a lack of equity in socioeconomic factors. The outbreak of viral infections such as Coronavirus Disease 2019 (COVID-19) [10], which initially started as a pandemic, and the outbreak of Monkeypox (Mpox), which has been

*Corresponding author: ezefrankline@imsuonline.edu.ng

a global threat, has clearly illustrated how quickly emerging/re-emerging infections can compromise healthcare infrastructure, as well as threaten social and economic functioning. Although a lot has been invested in exploring, studying, and managing a particular infectious disease, the rising cases of concurrent epidemics have occupied a renewed position in relevance on the matter of co-infection.

The COVID-19 pandemic, which is attributed to the Severe Acute Respiratory Syndrome Coronavirus 2 (SARS-CoV-2), broke out in Wuhan, China, at the end of December 2019, with the World Health Organization declaring it a global pandemic in March 2020 [48]. Despite the accelerated development, distribution, and implementation of vaccine and treatment technologies, the COVID-19 pandemic remains a global problem owing to factors such as genetic variations, immunity decline, reinfection, as well as inequalities in accessing vaccines, among others [1, 3, 10]. The Monkeypox disease, which is a zoonotic viral disease caused by the Monkeypox virus, has been considered endemic within Central and West Africa. Recent cases within non-endemic areas, however, have revealed the potential for this disease to also become a problem of high relevance within the said communities, especially among those in close contact [6, 2].

Co-infection refers to a situation where a host is infected by two or more pathogens, which might result in host-pathogen interactions that affect disease trajectories, host responses, or even transmissibility [16, 7, 8]. In the case of COVID-19, the Monkeypox outbreak, as well as other infections, co-infection challenges can worsen host conditions, especially in susceptible individuals such as immunocompromised patients [5]. The host-pathogen interactions, therefore, emphasize the need to analyze host-pathogen interactions within co-infections as opposed to handling infections such as COVID-19, especially within the context of the Monkeypox outbreak, separately.

infectious disease spread and the efficiency of different intervention methods. Compartment models, introduced by [9, 4], have been extensively used for studying infectious disease spread and control. Compartment models make it possible to divide a population into different compartments that are significant from the perspective of disease spread, thereby making it possible to assess different interventions such as vaccines, isolation, treatment, and behavior changes [11, 31]. In the context of the COVID-19 outbreak, a large number of mathematical models have been used to analyze disease transmission, nonpharmaceutical interventions, and vaccines [12, 13, 26, 38]. In a similar manner, models for Monkeypox outbreak have been used to analyze disease spillover, human-to-human transmission, isolation, and vaccines [14, 15]. Despite such progress, research on modeling COVID-19, Monkeypox, together with their co-infection, is still scant. This is because modeling co-infections is inherently more complicated due to interactions with nonlinearities, common control interventions, and multiple channels of transmission. The starting part of this work, therefore, filled this research gap by developing a deterministic compartmental model that includes interventions such as vaccination, quarantine, treatment, reinfection, as well as co-infection of COVID-19 and Monkeypox. The well-posedness, reproduction numbers, together with the local and global stability of disease-free and endemic equilibrium points were shown to be mathematically sound. Although theoretical findings are significant from a qualitative perspective, computational analysis is necessary for a deeper comprehension of the quantitative aspects of complicated epidemiological models. Computer simulations facilitate the evaluation of real-life scenarios that are dif-

ficult to analyze qualitatively, thereby providing the means to examine the efficiency of control interventions, which vary with the set of parameters [17, 18]. Sensitivity analysis is a significant application that helps define the most influential parameters of disease spread and survival. Besides sensitivity analysis, another useful technique employed for designing cost-effective intervention tactics in handling infectious diseases is the theory of optimal control. This theory uses optimal control models with time-dependent control variables that denote different public health interventions aimed at optimizing the reduction of disease prevalence, alongside the cost of implementation [19, 21]. The use of the theory of optimal control has been considered successful in handling various types of diseases such as HIV, TB, Malaria, and COVID-19. The use of the theory on multi-disease co-infection models, especially with emerging infections such as COVID-19 and Monkeypox, has not been extensively investigated.

In this continuation of the research [16], emphasis is placed on the numerical analysis and control-oriented analysis of the COVID-19-Monkeypox co-infection model. The positivity of solutions is mathematically justified via the application of the Laplace transform technique, ensuring that all state variables are non-negative. The existence and uniqueness of solutions are also demonstrated, providing a rigorous mathematical basis for the conducted numerical simulations. Sensitivity analysis on the basic reproduction numbers of the COVID-19 pandemic and the Monkeypox disease outbreak is performed using normalized forward sensitivity indices, making it possible to identify major parameters that affect disease transmission. Additionally, an optimal control problem is set to examine the cumulative impact of vaccines, quarantine, and treatment interventions on the reduction of disease cases, as well as the accumulated costs.

Research Gaps. Despite the rising literature on COVID-19 [49] and Monkeypox, a number of significant research gaps still exist. Firstly, there is a lack of a comprehensive COVID-19 and Monkeypox co-infection model that considers the effects of vaccines, quarantine, treatment, reinfection, and various interactions altogether. Secondly, little research has been conducted to validate the models mathematically, especially concerning the positivity, existence, and uniqueness of the solutions of the models. Thirdly, very limited research has been pursued concerning the sensitivity analysis of the models. Lastly, the application of optimal control models within a co-infection setting with respect to cost-effective, time-evolving controls remains an untouched research area. This study extends [16], which established the COVID-19–Monkeypox co-infection model, including its formulation, basic properties, reproduction numbers, and stability analyses of both disease-free and endemic equilibria. However, key aspects were not addressed. This work fills those gaps by conducting a sensitivity analysis of the basic reproduction numbers for both diseases, developing an optimal control framework for intervention strategies, and performing numerical simulations to illustrate and validate the model dynamics.

2. Description of Model

This study develops a deterministic compartmental model for the transmission dynamics of COVID-19 and Monkeypox co-infection in human and rodent populations. The human population $N_h(t)$ is subdivided into twelve compartments:

$$S_h,\ V_c,\ V_m,\ E_c^h,\ E_m^h,\ Q_c,\ Q_m,\ I_c^h,\ I_m^h,\ I_{cm}^h,\ T_h,\ R_h,$$

while the rodent population $N_r(t)$ consists of:

$$S_r,\ E_r,\ I_r.$$

Humans and rodents are recruited at rates Λ_h and Λ_r. Vaccination against COVID-19 and Monkeypox occurs at rates θ_c and θ_m, with vaccine failure rates ψ_c and ψ_m. Human-to-human transmission occurs at rates β_c (COVID-19) and β_m (Monkeypox), rodent-to-human Monkeypox transmission at rate β_1, and rodent-to-rodent transmission at rate β_r.

Exposed humans progress to infectious classes at rates α_c^1 and α_m^1, or enter quarantine at rates α_c^2 and α_m^2. Exposed rodents progress to infection at rate α_r. Quarantined COVID-19 individuals recover naturally at rate σ, while Monkeypox has no natural recovery in quarantine. Symptomatic quarantined individuals move to treatment at rates ζ_c and ζ_m.

Infected individuals may enter treatment at rates γ_c and γ_m, or develop co-infection at rate π. Co-infected individuals enter treatment at rate γ_{cm} or recover from either disease at rates τ_m and τ_c. Treated individuals recover at rate ϕ. Natural mortality rates for humans and rodents are μ_h and μ_r, while disease-induced mortalities are δ_c, δ_m, and δ_{cm}. Mortality is reduced in treatment by modification parameter η.

Recovered individuals may be reinfected with COVID-19 at rates χ (post-recovery) and ω (due to waning immunity).

The forces of infection are given by:

$$\lambda_c(t) = \frac{\beta_c(I_c^h + I_{cm}^h)}{N_h}, \qquad \lambda_m(t) = \frac{\beta_1 I_r + \beta_m(I_m^h + I_{cm}^h)}{N_h}, \qquad \lambda_r(t) = \frac{\beta_r I_r}{N_r}.$$

The total population is:

$$N_h(t) = S_h + V_c + V_m + E_c^h + E_m^h + Q_c + Q_m + I_c^h + I_m^h + I_{cm}^h + T_h + R_h,$$

$$N_r(t) = S_r + E_r + I_r.$$

2.1. Model Differential equation Referenced from Previous Work [16]

$$
\begin{aligned}
\frac{dS_h}{dt} &= \Lambda_h + \psi_c V_c + \psi_m V_m + \omega R_h - (\theta_c + \theta_m + \lambda_c + \lambda_m + \mu_h)\, S_h \\
\frac{dV_c}{dt} &= \theta_c S_h - (\psi_c + \mu_h) V_c \\
\frac{dV_m}{dt} &= \theta_m S_h - (\psi_m + \mu_h) V_m \\
\frac{dE_c^h}{dt} &= \lambda_c S_h - (\alpha_c^1 + \alpha_c^2 + \mu_h) E_c^h \\
\frac{dE_m^h}{dt} &= \lambda_m S_h - (\alpha_m^1 + \alpha_m^2 + \mu_h) E_m^h \\
\frac{dQ_c}{dt} &= \alpha_c^2 E_c^h - (\zeta_c \rho + \sigma + \mu_h) Q_c \\
\frac{dQ_m}{dt} &= \alpha_m^2 E_m^h - (\zeta_m \rho + \mu_h) Q_m \\
\frac{dI_c^h}{dt} &= \alpha_c^1 E_c^h + \chi \lambda_c R_h + \tau_m I_{cm}^h - (\pi \lambda_m + \gamma_c + \mu_h + \delta_c) I_c^h \\
\frac{dI_m^h}{dt} &= \alpha_m^1 E_m^h + \tau_c I_{cm}^h - (\pi \lambda_c + \gamma_m + \mu_h + \delta_m) I_m^h \\
\frac{dI_{cm}^h}{dt} &= \pi \lambda_m I_c^h + \pi \lambda_c I_m^h - (\tau_m + \tau_c + \gamma_{cm} + \mu_h + \delta_{cm}) I_{cm}^h \\
\frac{dT_h}{dt} &= \zeta_c \rho Q_c + \zeta_m \rho Q_m + \gamma_c I_c^h + \gamma_m I_m^h + \gamma_{cm} I_{cm}^h - (\phi + \mu_h + \eta \delta_t) T_h \\
\frac{dR_h}{dt} &= \phi T_h + \sigma Q_c - (\chi \lambda_c + \omega + \mu_h) R_h \\
\frac{dS_r}{dt} &= \Lambda_r - (\lambda_r + \mu_r) S_r \\
\frac{dE_r}{dt} &= \lambda_r S_r - (\alpha_r + \mu_r) E_r \\
\frac{dI_r}{dt} &= \alpha_r E_r - \mu_r I^r
\end{aligned}
\tag{2.1}
$$

where

$$
\begin{aligned}
\lambda_c(t) &= \frac{\beta_c (I_c^h + I_{cm}^h)}{N_h} \\
\lambda_m(t) &= \frac{\beta_1 I_r + \beta_m (I_m^h + I_{cm}^h)}{N_h}; \\
\lambda_r(t) &= \frac{\beta_r I_r}{N_r(t)}
\end{aligned}
$$

.

Based on previous research [16] the variables and parameters of the work are outlined bellow:

2.0

Table 1: Model Variables and description.

Variables	**Description**
S_h	Susceptible humans population
S_r	Susceptible rodents population
V_c	Covid-19 Vaccinated individuals
V_m	Monkeypox Vaccinated individuals
E_c^h	Exposed human Covid-19 Population
E_m^h	Exposed human Monkeypox Population
E_r	Exposed rodents population to Monkeypox
Q_c	Quarantined COVID-19 population
Q_m	Quarantined Monkeypox population
I_c^h	Infected COVID-19 Population
I_m^h	Infected Monkeypox Population
I_{cm}^h	Monkeypox and COVID-19 coinfected population
I_r	Infected rodents population
T_h	Treatment Class of humans
R_h	Individuals who have recovered from monkeypox, covid-19 and co- infections

Table 2: Model parameters and description.

Parameter	Description
Λ_h	Recruitment rate for humans
Λ_r	Recruitment rate for rodents
β_c	Transmission rate of susceptible humans from infected COVID-19 humans
β_m	Transmission rate of susceptible humans from infected Monkeypox humans
β_r	Transmission rate of susceptible rodents from infected rodents
β_1	Transmission rate of susceptible humans from infected rodents
λ_c	Force of infection for COVID-19 infection
λ_m	Force of infection for Monkeypox infection
λ_r	Force of infection for rodents
α_c^1	Progression rate from exposed COVID-19 individuals to infectious COVID-19 humans
α_c^2	Progression rate from exposed COVID-19 individuals to quarantined COVID-19 humans
α_m^1	Progression rate from exposed Monkeypox individuals to infectious Monkeypox humans
α_m^2	Progression rate from exposed Monkeypox individuals to quarantined Monkeypox humans
α_r	Progression rate from exposed rodents to infectious rodents
θ_c	Vaccination rate for COVID-19
θ_m	Vaccination rate for Monkeypox
ψ_c	COVID-19 vaccine failure rate
ψ_m	Monkeypox vaccine failure rate
ζ_c	Treatment rate of quarantined COVID-19 individuals
ζ_m	Treatment rate of quarantined Monkeypox individuals
ρ	Rate of developing clinical symptoms during quarantine
τ_c	COVID-19 recovery rate for co-infected individuals
τ_m	Monkeypox recovery rate for co-infected individuals
π	Increased susceptibility to infection as a result of underlying sickness (COVID-19/Monkeypox)
σ	COVID-19 natural recovery rate
γ_c	Treatment rate of infected COVID-19 individuals
γ_m	Treatment rate of infected Monkeypox individuals
γ_{cm}	Treatment rate of co-infected COVID-19 and Monkeypox individuals
ϕ	Recovery rate of treated individuals
χ	Increased infectiousness of COVID-19 recovered individuals
δ_c	COVID-19 induced death rate
δ_m	Monkeypox induced death rate
δ_{cm}	Co-infected induced death rate
η	Modification parameter that accounts for reduced death rate in the treatment class
μ_h	Natural death rate for humans
μ_r	Natural death rate for rodents
ω	Rate at which individuals lose immunity

3. Results and Analysis of the Model

In this chapter, we present the analysis and results of the model, which include the investigation of the existence and uniqueness of the solution using the fixed point theorem, optimal control analysis, sensitivity analysis of the basic reproduction numbers for both diseases, and numerical simulations implemented using Python software.

3.1. Basic reproduction Numbers

The basic reproduction number has been obtained from previous research [16], we have

$$R_0 = \max\left(\frac{\beta_c S_h^0 \alpha_c^1}{N_h^0 k_1 k_5}, \frac{\beta_m S_h^0 \alpha_m^1}{N_h^0 k_2 k_6}, \frac{\beta_r \alpha_r}{k_8 \mu_r}\right)$$

where

$$k_1 = \alpha_c^1 + \alpha_c^2 + \mu_h, \quad k_2 = \alpha_m^1 + \alpha_m^2 + \mu_h, \quad k_3 = \zeta_c \rho + \sigma + \mu_h, \quad k_4 = \zeta_m \rho + \mu_h,$$
$$k_5 = \gamma_c + \mu_h + \delta_c, \quad k_6 = \gamma_m + \mu_h + \delta_m, \quad k_7 = \tau_m + \tau_c + \gamma_{cm} + \mu_h + \delta_{cm}, \quad k_8 = \alpha_r + \mu_r.$$

3.2. Optimal Control Strategy to Reducing the Diseases Burden

We introduce four control variables, each a function of time t and bounded between 0 (no intervention) and 1 (maximum effort):

The time-dependent control variables $u_i(t) \in [0,1]$ for $i = 1,2,3,4$ are defined as follows:

- $\mathbf{u_1(t)}$: **COVID-19 Vaccination Control.** This represents the effort to increase the vaccination rate θ_c.
- $\mathbf{u_2(t)}$: **Monkeypox Vaccination Control.** This represents the effort to increase the vaccination rate θ_m.
- $\mathbf{u_3(t)}$: **Quarantine Control.** This represents the effort to identify and quarantine exposed individuals, increasing the rates α_c^2 and α_m^2.
- $\mathbf{u_4(t)}$: **Treatment Control.** This represents the effort to provide treatment, increasing the recovery rates γ_c, γ_m, γ_{cm}, ζ_c, ζ_m and potentially reducing death rates.

Using these controls, the Co-infection model (2.1) with optimal control now Modifies into:

$$
\begin{aligned}
\frac{dS_h}{dt} &= \Lambda_h + \psi_c V_c + \psi_m V_m + \omega R_h \\
&\quad - \left((\theta_c + u_1(t)) + (\theta_m + u_2(t)) + \frac{\beta_c (I_c^h + I_{cm}^h)}{N_h} + \frac{\beta_1 I_r^m + \beta_m (I_m^h + I_{cm}^h)}{N_h} + \mu_h \right) S_h \\
\frac{dV_c}{dt} &= (\theta_c + u_1(t)) S_h - \psi_c V_c - \mu_h V_c \\
\frac{dV_m}{dt} &= (\theta_m + u_2(t)) S_h - \psi_m V_m - \mu_h V_m \\
\frac{dE_c^h}{dt} &= \frac{\beta_c (I_c^h + I_{cm}^h)}{N_h} S_h - (\alpha_c^1 + (\alpha_c^2 + u_3(t)) + \mu_h) E_c^h \\
\frac{dE_m^h}{dt} &= \frac{\beta_1 I_r^m + \beta_m (I_m^h + I_{cm}^h)}{N_h} S_h - (\alpha_m^1 + (\alpha_m^2 + u_4(t)) + \mu_h) E_m^h \\
\frac{dQ_c}{dt} &= \alpha_c^2 E_c^h - ((\zeta_c + u_4(t))\rho + \sigma + \mu_h) Q_c \\
\frac{dQ_m}{dt} &= \alpha_m^2 E_m^h - ((\zeta_m + u_4(t))\rho + \mu_h) Q_m \\
\frac{dI_c^h}{dt} &= \alpha_c^1 E_c^h + \chi \frac{\beta_c (I_c^h + I_{cm}^h)}{N_h} R_h + \tau_m I_{cm}^h - \left(\pi \frac{\beta_1 I_r^m + \beta_m (I_m^h + I_{cm}^h)}{N_h} + (\gamma_c + u_4(t)) + \mu_h + \delta_c \right) I_c^h \\
\frac{dI_m^h}{dt} &= \alpha_m^1 E_m^h + \tau_c I_{cm}^h - \left(\pi \frac{\beta_c (I_c^h + I_{cm}^h)}{N_h} + (\gamma_m + u_4(t)) + \mu_h + \delta_m \right) I_m^h \\
\frac{dI_{cm}^h}{dt} &= \pi \frac{\beta_1 I_r^m + \beta_m (I_m^h + I_{cm}^h)}{N_h} I_c^h + \pi \frac{\beta_c (I_c^h + I_{cm}^h)}{N_h} I_m^h - (\tau_m + \tau_c + (\gamma_{cm} + u_4(t)) + \mu_h + \delta_{cm}) I_{cm}^h \\
\frac{dT_h}{dt} &= (\zeta_c \rho + u_4(t)) Q_c + (\zeta_m \rho + u_4(t)) Q_m \\
&\quad + (\gamma_c + u_4(t)) I_c^h + (\gamma_m + u_4(t)) I_m^h + (\gamma_{cm} + u_4(t)) I_{cm}^h - (\phi + \mu_h + \eta \delta_t) T_h \\
\frac{dR_h}{dt} &= \phi T_h + \sigma Q_c - \left(\chi \frac{\beta_c (I_c^h + I_{cm}^h)}{N_h} + \omega + \mu_h \right) R_h \\
\frac{dS_r}{dt} &= \Lambda_r - \left(\frac{\beta_r I_r}{N_r} + \mu_r \right) S_r \\
\frac{dE_r}{dt} &= \frac{\beta_r I_r}{N_r} S_r - (\alpha_r + \mu_r) E_r \\
\frac{dI_r}{dt} &= \alpha_r E_r - \mu_r I^r
\end{aligned}
\tag{3.1}
$$

Define the cost functional:

$$
\begin{aligned}
&J(u_1, u_2, u_3, u_4) \\
&= \int_0^t \left[A_1 I_c^h(t) + A_2 I_m^h(t) + A_3 I_{cm}^h(t) + A_4 Q_c(t) + A_5 Q_m(t) + \frac{1}{2}(B_1 u_1^2 + B_2 u_2^2 + B_3 u_3^2 + B_4 u_4^2) \right] dt
\end{aligned}
\tag{3.2}
$$

In this context, the variables (A_i) where $(i = 1, 2, 3, 4, 5)$ represent the weight constants that quantify the cost (social, economic, health burden) of having individuals in the infected I and quarantined Q compartments, while the variables (B_i) where $(i = 1, 2, 3, 4)$ denote the weight constants that reflect the relative cost of implementing each intervention. The quadratic term $(B_i)u_i^2(t)$ is used to model the non-linear cost of intervention effort The goal is to minimize J subject to the dynamics of the system. Let U be the set of all admissible control functions defined over the finite time interval $[0, T]$.
The controls must satisfy three mathematical properties:

1. **Lebesgue measurable:**
   This ensures the control function is well-defined for almost every time t. It prevents controls from being too irregular or discontinuous.
2. **Essentially bounded ($L^\infty(0, T)$):** This means the control function does not become infinitely large. There exists a constant M such that $|u(t)| \leqslant M$
3. **Takes values in** $[0, 1]$**:** The control lies between 0 and 1

Then, Putting these together

$$U = \left\{ (u) \in [L^\infty(0, T)]^4 \;\middle|\; 0 \leqslant u(t) \leqslant 1 \text{ for all } t \in [0, T] \right\}, \text{ for all controls } u(t).$$

3.2.1. Construct the Hamiltonian of optimal control

We are applying Pontryagin's Maximum Principle (PMP) to find the optimal control functions

$$u_1(t),\ u_2(t),\ u_3(t),\ u_4(t)$$

that minimize the cost functional while respecting the system dynamics.

PMP states that, to solve an optimal control problem, we must construct the Hamiltonian, defined as:

$$\mathcal{H}(x, u, \lambda) = (\text{instantaneous cost}) + \sum_{i=1}^{15} \lambda_i f_i(x, u),$$

where:

- x = state variables,
- u = control variables,
- $\lambda_i(t)$ = adjoint (costate) variables,
- $f_i(x, u)$ = right-hand side of the ODE for the i-th state variable.

Construct the Hamiltonian $\mathcal{H}$

$$\begin{aligned}
\mathcal{H} = {} & A_1 I_c^h + A_2 I_m^h + A_2 I_{cm}^h + A_4 Q_c + A_5 Q_m + \frac{1}{2}\left[B_1 u_1^2(t) + B_2 u_2^2(t) + B_3 u_3^2(t) + B_4 u_4^2(t)\right] \\
& + \lambda_1\left[\Lambda_h + \psi_c V_c + \psi_m V_m + \omega R_h - \left((\theta_c + u_1(t)) + (\theta_m + u_2(t))\right.\right. \\
& \left.\left. + \frac{\beta_c(I_c^h + I_{cm}^h)}{N_h} + \frac{\beta_1 I_r^m + \beta_m(I_m^h + I_{cm}^h)}{N_h} + \mu_h\right) S_h\right] \\
& + \lambda_2\left[(\theta_c + u_1(t))S_h - \psi_c V_c - \mu_h V_c\right] \\
& + \lambda_3\left[(\theta_m + u_2(t))S_h - \psi_m V_m - \mu_h V_m\right] \\
& + \lambda_4\left[\frac{\beta_c(I_c^h + I_{cm}^h)}{N_h} S_h - (\alpha_c^1 + (\alpha_c^2 + u_3(t)) + \mu_h) E_c^h\right] \\
& + \lambda_5\left[\frac{\beta_1 I_r^m + \beta_m(I_m^h + I_{cm}^h)}{N_h} S_h - (\alpha_m^1 + (\alpha_m^2 + u_4(t)) + \mu_h) E_m^h\right] \\
& + \lambda_6\left[\alpha_c^2 E_c^h - ((\zeta_c + u_4(t))\rho + \sigma + \mu_h) Q_c\right] \\
& + \lambda_7\left[\alpha_m^2 E_m^h - ((\zeta_m + u_4(t))\rho + \mu_h) Q_m\right] \\
& + \lambda_8\left[\alpha_c^1 E_c^h + \chi\frac{\beta_c(I_c^h + I_{cm}^h)}{N_h} R_h + \tau_m I_{cm}^h - \left(\pi\frac{\beta_1 I_r^m + \beta_m(I_m^h + I_{cm}^h)}{N_h} + (\gamma_c + u_4(t)) + \mu_h + \delta_c\right) I_c^h\right] \\
& + \lambda_9\left[\alpha_m^1 E_m^h + \tau_c I_{cm}^h - \left(\pi\frac{\beta_c(I_c^h + I_{cm}^h)}{N_h} + (\gamma_m + u_4(t)) + \mu_h + \delta_m\right) I_m^h\right] \\
& + \lambda_{10}\left[\pi\frac{\beta_1 I_r^m + \beta_m(I_m^h + I_{cm}^h)}{N_h} I_c^h + \pi\frac{\beta_c(I_c^h + I_{cm}^h)}{N_h} I_m^h - (\tau_m + \tau_c + (\gamma_{cm} + u_4(t)) + \mu_h + \delta_{cm}) I_{cm}^h\right] \\
& + \lambda_{11}\left[(\zeta_c\rho + u_4(t))Q_c + (\zeta_m\rho + u_4(t))Q_m + (\gamma_c + u_4(t))I_c^h\right. \\
& \left. + (\gamma_m + u_4(t))I_m^h + (\gamma_{cm} + u_4(t))I_{cm}^h - (\phi + \mu_h + \eta\delta_t)T_h\right] \\
& + \lambda_{12}\left[\phi T_h + \sigma Q_c - \left(\chi\frac{\beta_c(I_c^h + I_{cm}^h)}{N_h} + \omega + \mu_h\right) R_h\right] \\
& + \lambda_{13}\left[\Lambda_r - \left(\frac{\beta_r I_r}{N_r(t)} + \mu_r\right) S_r\right] \\
& + \lambda_{14}\left[\frac{\beta_r I_r}{N_r(t)} S_r - (\alpha_r + \mu_r) E_r\right] \\
& + \lambda_{15}\left[\alpha_r E_r - \mu_r I_r\right]
\end{aligned}$$

By applying Pontryagin's maximum principle and utilizing the existence result for optimal control pairs $(u_1^*(t), u_2^*(t), u_3^*(t), u_4^*(t)$, the theorem is established. Here, $\lambda_i (i = 1, 2, 3, ...15)$ denotes the adjoint functions that are linked to the model's state variables.

3.2.2. Derive Adjoint Equations of optimal control

Theorem 3.1. *There exist an optimal control pairs* $u_1^*(t), u_2^*(t), u_3^*(t)$, *and* u_4^* *corresponding solution*
$(S_h^*, V_c^*, V_m^*, E_c^{h*}, E_m^{h*}, Q_c^*, Q_m^*, I_c^{h*}, I_m^{h*}, I_{cm}^{h*}, T_h^*, R_h^*, S_r^*, E_r^*, I_r^*)$ *that minimize*
$J(u_1^*(t), u_2^*(t), u_3^*(t), u_4^*(t)$ *over* D. *Furthermore, there exist adjoint function,* $\lambda_i (i = 1, 2, 3, ...15)$ *such that:*

To differentiate λ_1 with respect to time t, we must utilize Pontryagin's Maximum Principle. In the context of optimal control problems, the adjoint (costate) equations are obtained by calculating the negative partial derivative of the Hamiltonian
$\mathcal{H}$ with respect to the relevant state variable.

$$\frac{d\lambda_1}{dt} = -\frac{\partial \mathcal{H}}{\partial S_h}$$

This gives a system of n adjoint equations (for each state variable). We now find all the terms in the Hamiltonian $\mathcal{H}$ that contain S_h and compute the partial derivative of $\mathcal{H}$ with respect to S_h

The adjoint variable λ_1 satisfies the differential equation:

$$\frac{d\lambda_1}{dt} = -\frac{\partial H}{\partial S_h}$$

where H is the Hamiltonian. Computing the partial derivative:

Therefore, Combine all the partial derivatives, we have

$$\frac{d\lambda_1}{dt} = -\frac{\partial H}{\partial S_h} = \lambda_1 \left((\theta_c + u_1(t)) + (\theta_m + u_2(t)) + \frac{\beta_c (I_c + I_{cm})}{N_h} + \beta_1 I_r + \frac{\beta_m (I_m + I_{cm})}{N_h} + \mu_h \right)$$
$$-\lambda_2(\theta_c + u_1(t)) - \lambda_3(\theta_m + u_2(t)) - \lambda_4 \frac{\beta_c (I_c + I_{cm})}{N_h} - \lambda_5 \frac{\beta_m (I_m + I_{cm})}{N_h}$$

The adjoint variable λ_2 satisfies the differential equation:

$$\frac{d\lambda_2}{dt} = -\frac{\partial H}{\partial V_c}$$

where H is the Hamiltonian. Computing the partial derivative:

$$\frac{\partial H}{\partial V_c} = \lambda_1 \Psi_c + \lambda_2(-\Psi_c - \mu_h)$$

Therefore,

$$\frac{d\lambda_2}{dt} = -\frac{\partial H}{\partial V_c} = -\left[\lambda_1 \Psi_c - \lambda_2(\Psi_c + \mu_h)\right] = \lambda_2(\Psi_c + \mu_h) - \lambda_1 \Psi_c$$

The adjoint variable λ_3 satisfies the differential equation:

$$\frac{d\lambda_3}{dt} = -\frac{\partial H}{\partial V_m}$$

where H is the Hamiltonian. Computing the partial derivative: Therefore,

$$\frac{d\lambda_3}{dt} = -\frac{\partial H}{\partial V_m} = -\left[\lambda_1\Psi_m - \lambda_3(\Psi_m + \mu_h)\right] = \lambda_3(\Psi_m + \mu_h) - \lambda_1\Psi_m$$

The adjoint variable λ_4 satisfies the differential equation:

$$\frac{d\lambda_4}{dt} = -\frac{\partial H}{\partial E_c}$$

where H is the Hamiltonian. Computing the partial derivative:

The terms containing E_c in the Hamiltonian are:

Therefore:

$$\begin{aligned}\frac{d\lambda_4}{dt} = -\frac{\partial H}{\partial E_c} &= -\left[-\lambda_4(\alpha_c^1 + (\alpha_c^2 + u_3(t)) + \mu_h) + \lambda_6(\alpha_c^2 + u_3(t)) + \lambda_8\alpha_c^1\right] \\ &= \lambda_4(\alpha_c + (\alpha_c^2 + u_3(t)) + \mu_h) - \lambda_6(\alpha_c^2 + u_3(t)) - \lambda_8\alpha_c^1\end{aligned}$$

The adjoint variable λ_5 satisfies the differential equation:

$$\frac{d\lambda_5}{dt} = -\frac{\partial H}{\partial E_m}$$

where H is the Hamiltonian. Computing the partial derivative:

The terms containing E_m in the Hamiltonian are:

$$\begin{aligned}\frac{d\lambda_5}{dt} = -\frac{\partial H}{\partial E_m} &= -\left[-\lambda_5(\alpha_m + (\alpha_m^2 + u_3(t)) + \mu_h) + \lambda_7(\alpha_m^2 + u_3(t)) + \lambda_9\alpha_m^1\right] \\ &= \lambda_5(\alpha_m^1 + (\alpha_m^2 + u_3(t)) + \mu_h) - \lambda_7(\alpha_m^2 + u_3(t)) - \lambda_9\alpha_m^1\end{aligned}$$

The adjoint variable λ_6 satisfies the differential equation:

$$\frac{d\lambda_6}{dt} = -\frac{\partial H}{\partial Q_c}$$

where H is the Hamiltonian. Computing the partial derivative:

The terms containing Q_c in the Hamiltonian are:

$$\begin{aligned}\frac{d\lambda_6}{dt} = -\frac{\partial H}{\partial Q_c} &= -\left[-\lambda_6((\zeta_c\rho + u_4(t)) + \sigma + \mu_h) + \lambda_{11}(\zeta_c\rho + u_4(t)) + \lambda_{12}\sigma\right] \\ &= \lambda_6((\zeta_c\rho + u_4(t)) + \sigma + \mu_h) - \lambda_{11}(\zeta_c\rho + u_4(t)) - \lambda_{12}\sigma\end{aligned}$$

The adjoint variable λ_7 satisfies the differential equation:

$$\frac{d\lambda_7}{dt} = -\frac{\partial H}{\partial Q_m}$$

where H is the Hamiltonian. Computing the partial derivative:

The terms containing Q_m in the Hamiltonian are:

$$\frac{d\lambda_7}{dt} = -\frac{\partial H}{\partial Q_m} = -\left[-\lambda_7((\zeta_m\rho + u_4(t)) + \mu_h) + \lambda_{11}(\zeta_m\rho + u_4(t))\right]$$
$$= \lambda_7((\zeta_m\rho + u_4(t)) + \mu_h) - \lambda_{11}(\zeta_m\rho + u_4(t))$$

The adjoint variable λ_8 satisfies the differential equation:

$$\frac{d\lambda_8}{dt} = -\frac{\partial H}{\partial I_c}$$

where H is the Hamiltonian. Computing the partial derivative:

Therefore:

$$\frac{d\lambda_8}{dt} = -\frac{\partial H}{\partial I_c} = \lambda_1\frac{\beta_c}{N_h}S_h - \lambda_4\frac{\beta_c}{N_h}S_h + \lambda_8\left(\pi\beta_1 I_r + \frac{\beta_m(I_m + I_{cm})}{N_h} + (\gamma_c + u_4(t)) + \mu_h + \delta_c\right)$$
$$+\lambda_9\pi\frac{\beta_c}{N_h}I_m - \lambda_{10}\left(\pi\beta_1 I_r + \frac{\beta_m(I_m + I_{cm})}{N_h}\right) - \lambda_{11}(\gamma_c + u_4(t)) + \lambda_{12}\chi\frac{\beta_c}{N_h}R$$

The adjoint variable λ_9 satisfies the differential equation:

$$\frac{d\lambda_9}{dt} = -\frac{\partial H}{\partial I_m}$$

where H is the Hamiltonian. Computing the partial derivative:

Therefore:

$$\frac{d\lambda_9}{dt} = -\frac{\partial H}{\partial I_m} = \lambda_1\frac{\beta_m}{N_h}S_h - \lambda_5\frac{\beta_m}{N_h}S_h + \lambda_8\frac{\beta_m}{N_h}I_c + \lambda_9\left(\pi\frac{\beta_c(I_c + I_{cm})}{N_h} + (\gamma_m + u_4(t)) + \mu_h + \delta_m\right)$$
$$-\lambda_{10}\frac{\beta_m}{N_h}I_c - \lambda_{11}(\gamma_m + u_4(t)) + \lambda_{12}\chi\frac{\beta_c}{N_h}R$$

The adjoint variable λ_{10} satisfies the differential equation:

$$\frac{d\lambda_{10}}{dt} = -\frac{\partial H}{\partial I_{cm}}$$

where H is the Hamiltonian. Computing the partial derivative:

Therefore:

$$\frac{d\lambda_{10}}{dt} = -\frac{\partial H}{\partial I_{cm}} = \lambda_1\left(\frac{\beta_c}{N_h} + \frac{\beta_m}{N_h}\right)S_h - \lambda_4\frac{\beta_c}{N_h}S_h - \lambda_5\frac{\beta_m}{N_h}S_h - \lambda_8\left(\tau_m - \frac{\beta_m}{N_h}I_c\right)$$
$$-\lambda_9\left(\tau_c - \pi\frac{\beta_c}{N_h}I_m\right) - \lambda_{10}\left(\pi\lambda_c - (\tau_m + \tau_c + (\gamma_{cm} + u_4(t)) + \mu_h + \delta_{cm})\right) - \lambda_{11}(\gamma_{cm} + u_4(t)) + \lambda_{12}\chi\frac{\beta_c}{N_h}R$$

The adjoint variable λ_{11} satisfies the differential equation:

$$\frac{d\lambda_{11}}{dt} = -\frac{\partial H}{\partial T_h}$$

where H is the Hamiltonian. Computing the partial derivative:

The terms containing T_h in the Hamiltonian are:
Therefore:

$$\frac{d\lambda_{11}}{dt} = -\frac{\partial H}{\partial T_h} = -\left[-\lambda_{11}(\Phi + \mu_h + \sigma\delta_t) + \lambda_{12}\Phi\right] = \lambda_{11}(\Phi + \mu_h + \sigma\delta_t) - \lambda_{12}\Phi$$

The adjoint variable λ_{12} satisfies the differential equation:

$$\frac{d\lambda_{12}}{dt} = -\frac{\partial H}{\partial R}$$

where H is the Hamiltonian. Computing the partial derivative:
Therefore:

$$\frac{d\lambda_{12}}{dt} = -\frac{\partial H}{\partial R} = -\left[\lambda_1\omega + \lambda_8\chi\frac{\beta_c(I_c + I_{cm})}{N_h} - \lambda_{12}\left(\chi\frac{\beta_c(I_c + I_{cm})}{N_h} + \omega + \mu_h\right)\right]$$

$$= -\lambda_1\omega - \lambda_8\chi\frac{\beta_c(I_c + I_{cm})}{N_h} + \lambda_{12}\left(\chi\frac{\beta_c(I_c + I_{cm})}{N_h} + \omega + \mu_h\right)$$

The adjoint variable λ_{13} satisfies the differential equation:

$$\frac{d\lambda_{13}}{dt} = -\frac{\partial H}{\partial S_r}$$

where H is the Hamiltonian. Computing the partial derivative:
Therefore:

$$\frac{d\lambda_{13}}{dt} = -\frac{\partial H}{\partial S_r} = -\left[-\lambda_{13}\left(\frac{\beta_r I_r}{N_r} + \mu_r\right) + \lambda_{14}\frac{\beta_r I_r}{N_r}\right] = \lambda_{13}\left(\frac{\beta_r I_r}{N_r} + \mu_r\right) - \lambda_{14}\frac{\beta_r I_r}{N_r}$$

The adjoint variable λ_{14} satisfies the differential equation:

$$\frac{d\lambda_{14}}{dt} = -\frac{\partial H}{\partial E_r}$$

where H is the Hamiltonian. Computing the partial derivative:
The terms containing E_r in the Hamiltonian are:

$$\lambda_{14}\left[-(\alpha_r + \mu_r)E_r\right]$$
$$\lambda_{15}\left[\alpha_r E_r\right]$$

Thus:

$$\frac{\partial H}{\partial E_r} = \lambda_{14}(-(\alpha_r + \mu_r)) + \lambda_{15}\alpha_r$$
$$= -\lambda_{14}(\alpha_r + \mu_r) + \lambda_{15}\alpha_r$$

Therefore:

$$\frac{d\lambda_{14}}{dt} = -\frac{\partial H}{\partial E_r} = -\left[-\lambda_{14}(\alpha_r + \mu_r) + \lambda_{15}\alpha_r\right] = \lambda_{14}(\alpha_r + \mu_r) - \lambda_{15}\alpha_r$$

The adjoint variable λ_{15} satisfies the differential equation:

$$\frac{d\lambda_{15}}{dt} = -\frac{\partial H}{\partial I_r}$$

where H is the Hamiltonian. Computing the partial derivative:

Therefore:

$$\frac{d\lambda_{15}}{dt} = -\frac{\partial H}{\partial I_r} = \lambda_1\beta_1 - \lambda_5\beta_1 + \lambda_8\pi\beta_1 - \lambda_{10}\pi\beta_1 + \lambda_{13}\frac{\beta_r}{N_r}S_r - \lambda_{14}\frac{\beta_r}{N_r}S_r + \lambda_{15}\mu_r$$

This adjoint system completes the optimal control framework, allowing for the determination of time-dependent control strategies that minimize disease burden while considering economic costs and operational constraints.

3.2.3. Characterize the Optimal Controls

After applying Pontryagin's Maximum Principle, the optimal controls are obtained by differentiating the Hamiltonian with respect to each control variable. The resulting expressions may fall outside the allowed range of controls, so each control must be projected back into the admissible interval $[0,\ u_{j,max}]$.

This leads to the standard optimality characterization:

$$u_j^*(t) = \min\left\{u_{j,max},\ \max\{0,\ \text{unbounded control expression}\}\right\}.$$

From the Hamiltonian condition, the optimal control satisfies

$$\frac{\partial H}{\partial u_1} = 0 \quad \Rightarrow \quad u_1 = \frac{(\lambda_1 - \lambda_2)S_h}{B_1}.$$

This gives the **unbounded value** of u_1. However, in practice, controls are limited by operational constraints:

$$0 \leqslant u_1 \leqslant u_{1,max}.$$

Applying these constraints leads to the **bounded optimal control**:

$$u_1^*(t) = \min\left\{u_{1,max},\ \max\left\{0,\ \frac{(\lambda_1 - \lambda_2)S_h}{B_1}\right\}\right\}.$$

$$u_2^* = \min\left\{u_{2,max},\ \max\left\{0,\ \frac{(\lambda_1 - \lambda_3)S_h}{B_2}\right\}\right\}$$

$$u_3^*(t) = \min\left\{u_{3,max},\ \max\left(0,\ \frac{\lambda_4 E_c^h}{B_3}\right)\right\}.$$

$$u_4^* = \min\left\{u_{4,max},\ \max\left\{0,\ \frac{1}{B_4}\left[\lambda_5 E_m^h + \lambda_6\rho Q_c + \lambda_7\rho Q_m \right.\right.\right.$$
$$\left.\left.\left. + \lambda_8 I_c^h + \lambda_9 I_m^h + \lambda_{10} I_{cm}^h - \lambda_{11}(Q_c + Q_m + I_c^h + I_m^h + I_{cm}^h)\right]\right\}\right\}$$

The provided characterization is a powerful and theoretically sound result. It successfully translates a complex minimization problem into a set of actionable equations. The analysis demonstrates a deep understanding of optimal control theory and its application to epidemiology. The resulting control strategy is a sophisticated feedback policy that dynamically allocates resources based on the evolving population dynamics and the implicit "cost" of each individual's state.

3.3. Sensitivity Analysis of The Basic Reproduction Number of COVID-19 Only

The basic reproduction number for COVID-19, denoted as R_{0c}, depends on the parameters $\beta_c, \alpha_c^1, \alpha_c^2, \gamma_c, \delta_c,$, and μ_h. To manage the spread of the COVID-19 disease, these parameter values must be adjusted to ensure that R_0^c remains below one. Consequently, as the values of these parameters are modified, we can determine the rate of change of R_0^c. If we define $G_1 = (\beta_c, \alpha_c^1, \alpha_c^2, \gamma_c, \delta_c, \mu_h)$, then we can express the rate of change of R_0^c.

$$Z_{G_1}^{R_0^c} = \frac{\partial R_0^c}{\partial G_1} \times \frac{G_1}{R_0^c} \tag{3.3}$$

The normalized sensitivity index of the basic reproduction number with respect to $\alpha_c^1, \alpha_c^2, \gamma_c, \delta_c \pi, \mu_h$ is given by

Table 3: The Effect of the COVID-19 Parameters on R_0^c.

Parameters	**Baseline value**	$\frac{\partial R_0^c}{\partial p}(numeric)$	**Elasticity** $Z_p^{R_0^c}$	**Effect on** R_0^c
β_c	0.50 days	+5.3218	+1.0000	Positive
α_c^1	0.20 days	+3.4507	+0.2594	Positive
α_c^2	0.007 days	-9.8537	-0.2592	Negative
μ_h	0.000039 days	-43.7333	-0.000641	Negative
γ_c	0.075 days	-33.8797	-0.9549	Negative
δ_c	0.0035 days	-33.8797	-0.0446	Negative

Figure 1: Sensitivity Analysis of Basic Reproduction of COVID-19

Figure 4.3 presents the tornado plot of the elasticity of R_0^c to key model parameters. Green bars indicate parameters that increase R_0^c when increased, while red bars indicate parameters that reduce R_0^c. The COVID-19 transmission rate (β_c) has the highest positive elasticity (+1.00), making it the most influential parameter driving disease spread. Conversely, the treatment rate (γ_c) exhibits a strong negative elasticity (0.94), indicating that improved treatment and isolation significantly reduce transmission. The progression rate from exposed to infectious individuals (α_c^1) has a moderate positive effect (+0.26), whereas the quarantine rate of exposed individuals (α_c^2) has an equivalent negative effect (0.26), emphasizing the importance of early detection and quarantine. Disease-induced mortality (δ_c) and natural mortality (μ_h) have relatively small negative effects on R_0^c. Overall, the results show that reducing transmission, increasing treatment, and strengthening quarantine measures are the most effective strategies for controlling COVID-19.

Sustained improvements in these interventions can lower disease prevalence and reduce the likelihood of COVID-19–monkeypox coinfection, potentially driving the infection below the endemic threshold.

3.4. Sensitivity Analysis of The Basic Reproduction Number of Monkeypox Only

The sensitivity analysis of the basic reproduction number for the Monkeypox-only submodel aims to assess how variations in model parameters influence the transmission dynamics of monkeypox independently, while also considering the possible impact of coinfection. The basic reproduction number for monkeypox, represented as R_0^m, is influenced by the parameters $\beta_m, \alpha_m^1, \alpha_m^2, \gamma_m, \delta_m,$, and μ_h. To effectively control the spread of monkeypox, it is necessary to adjust these parameter values to keep R_0^m below one. By altering the values of these parameters, we can evaluate the change in R_0^m. If we let $G_2 = (\beta_m, \alpha_m^1, \alpha_m^2, \gamma_m, \delta_m, \mu_h)$, we can articulate the rate of change of R_0^m. Similarly,

$$Z_{G_2}^{R_0^m} = \frac{\partial R_0^m}{\partial G_2} \times \frac{G_2}{R_0^m} \tag{3.4}$$

The normalized sensitivity index of the basic reproduction number with respect to $\alpha_m^1, \alpha_m^2, \gamma_m, \delta_m, \mu_h$ is given by

Table 4: The Effect of the Monkeypox Parameters on R_0^m.

Parameters	**Baseline value**	$\frac{\partial R_0^m}{\partial p}(numeric)$	**Elasticity** $Z_p^{R_0^m}$	**Effect on** R_0^m
β_m	0.18 days	+19.3794	+1.000	Positive
α_m^1	0.085 days	+11.9791	+0.2919	Positive
α_m^2	0.035 days	-29.0596	-0.2916	Negative
μ_h	0.000039 days	-124.5272	-0.00139	Negative
γ_m	0.035 days	-95.4675	-0.9579	Negative
δ_m	0.0015 days	-95.4675	-0.04105	Negative

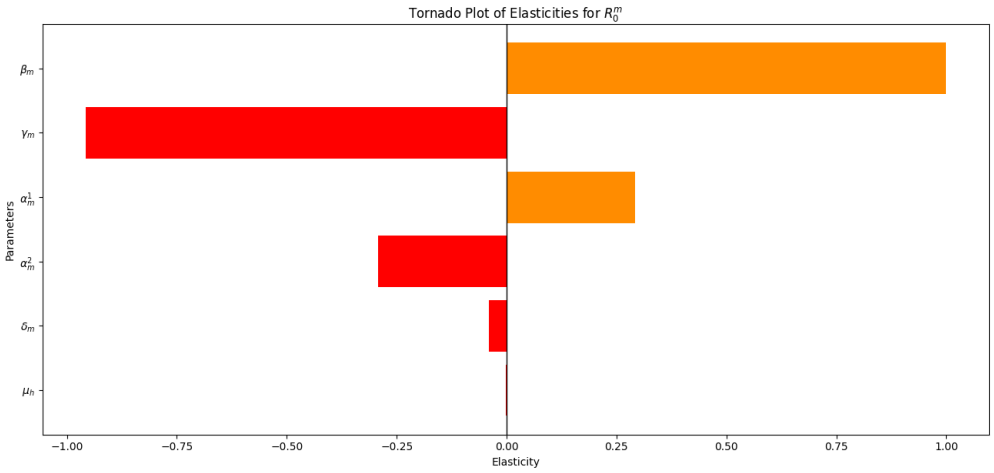

Figure 2: Sensitivity Analysis of Basic Reproduction of Monkeypox

Figure 4.4 presents the tornado plot of the elasticity of R_0^m to key model parameters. Dark orange bars represent parameters that increase R_0^m when increased, while red bars represent parameters that decrease R_0^m. The monkeypox transmission rate (β_m) has the highest positive elasticity (+1.00), indicating that reducing transmission is the most effective strategy for lowering disease spread. The treatment rate (γ_m) has the strongest negative elasticity (0.958), showing that improved treatment, recovery, and isolation substantially reduce R_0^m. The progression rate from exposed to infectious individuals (α_m^1) positively influences transmission (+0.292), whereas the quarantine rate of exposed individuals (α_m^2) has an equal but negative effect (0.292), highlighting the importance of early case detection and quarantine. Disease-induced mortality (δ_m) and natural mortality (μ_h) have relatively small negative effects on R_0^m. Overall, the results suggest that enhancing treatment and quarantine measures while reducing transmission can significantly lower monkeypox prevalence and help drive the disease below the endemic threshold.

3.5. Numerical Simulations and Discussions

Below, we present the graphs from our numerical simulations along with their corresponding interpretations. Initial values of the model state variables based on Florida population and outbreak data (CDC, WHO, Florida Health Department) as follows:

Figure 4.5 presents the simulation of COVID-19, monkeypox, and coinfection dynamics over 200 days. The logarithmic scale highlights differences in infection magnitudes. COVID-19 begins with a higher prevalence (8,000 cases) than monkeypox (250 cases) and reaches its peak earlier (days 40–50), reflecting its higher transmission and progression rates. Monkeypox peaks later (days 70–80), indicating distinct epidemiological characteristics. Coinfection cases remain comparatively low throughout the simulation, suggesting that simultaneous infection is uncommon but epidemiologically significant. The COVID-19 decline is driven by the reduction of susceptible individuals and the effects of interventions such as quarantine, treatment, and vaccination. The delayed monkeypox peak reflects its slower transmission dynamics. The co-infected class experiences higher

Table 5: Initial values of the model state variables based on Florida population and outbreak data.

Variable	Initial Value	Source
$S_h(0)$	2.1×10^7	[22]
$S_r(0)$	5.0×10^5	[27]
$V_c(0)$	1.5×10^7	[23]
$V_m(0)$	2.0×10^5	[28]
$E_c^h(0)$	1.5×10^3	[30]
$E_m^h(0)$	100	[32]
$E_r(0)$	200	[27]
$Q_c(0)$	2.0×10^3	[24]
$Q_m(0)$	80	[25]
$I_c^h(0)$	8.0×10^3	[30]
$I_m^h(0)$	250	[32]
$I_{cm}^h(0)$	10	[34]
$I_r(0)$	100	[27]
$T_h(0)$	50	[34]
$R_h(0)$	1.0×10^6	[24]

Table 6: Key epidemiological parameters of the co-infection model with their estimated values and sources.

Parameter	Value / Range	Source
Λ_h	5.8×10^2/day	[35]
Λ_r	2.7×10^2/day	[36]
β_c	0.3–0.7/day	[37]
β_m	0.12–0.25/day	[39]
β_r	0.08–0.15/day	[27]
β_1	0.05–0.1/day	[41]
α_c^1	0.15–0.25/day	[42]
α_m^1	0.07–0.1/day	[39]
α_r	0.05–0.1/day	[36]
θ_c	0.002–0.01/day	[43]
θ_m	0.0005–0.002/day	[28]
ψ_c	0.05–0.15	[44]
ψ_m	0.01–0.1	[40]
ζ_c	0.05–0.1/day	[29]
ζ_m	0.02–0.05/day	[33]
(τ_c, τ_m)	$(0.02-0.01, 0.05-0.03)$/day	[34]
σ	0.07/day	[45]
γ_c	0.05–0.1/day	[29]
γ_m	0.02–0.05/day	[33]
ϕ	0.05–0.1/day	[33]
δ_c	0.002–0.005/day	[30]
δ_m	0.001–0.002/day	[32]
δ_{cm}	0.01–0.02/day	[34]
μ_h	3.9×10^{-5}/day	[46]
μ_r	1.4×10^{-3}/day	[36]
ω	0.002–0.01/day	[47]

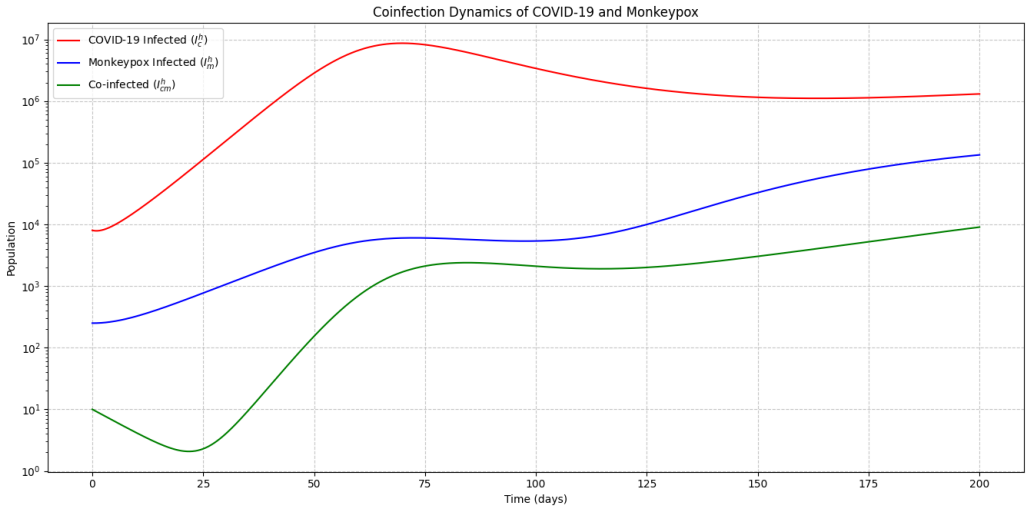

Figure 3: Simulation of Coinfection of the model

disease-induced mortality (δ_{cm}) and lower recovery rates (γ_{cm}), indicating the increased severity and treatment challenges associated with concurrent infections. Vaccinated compartments (V_c, V_m) reduce the susceptible population and contribute to herd immunity, while vaccine failure rates (ψ_c, ψ_m) account for imperfect protection and maintain residual transmission within the population. Figure 4.6 presents 3D surface plots showing the

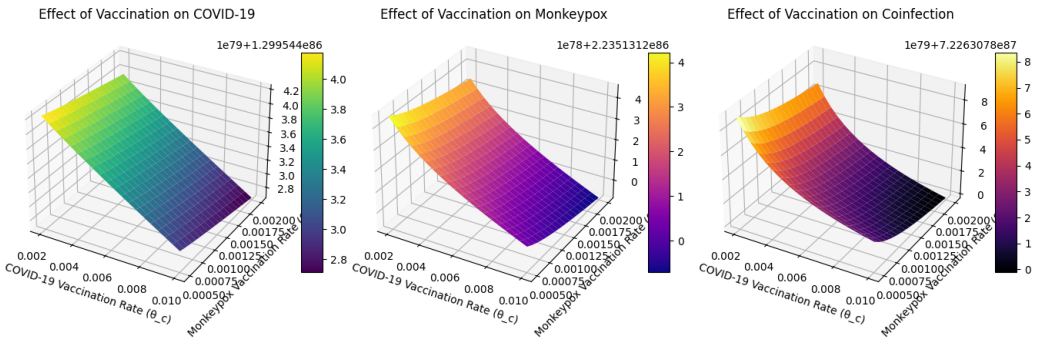

Figure 4: Effect of Vaccination rate on COVID-19, Monkeypox and Coinfection

effects of COVID-19 (θ_c) and monkeypox (θ_m) vaccination rates on the peak numbers of COVID-19, monkeypox, and coinfection cases over a 200-day simulation. As θ_c increases, peak COVID-19 infections decline markedly, while monkeypox vaccination has little effect on COVID-19 dynamics. Likewise, increasing θ_m significantly reduces monkeypox infections, with minimal influence from COVID-19 vaccination. The coinfection surface shows a reduction in cases as either vaccination rate increases, indicating that vaccination against either disease contributes to lowering coinfection burden. The results demon-

strate the effectiveness of vaccine-induced immunity in controlling disease transmission. However, the persistence of some monkeypox cases at high vaccination levels may reflect continued zoonotic transmission from infected rodents. Overall, the findings highlight the importance of coordinated vaccination strategies for both diseases, as modest increases in vaccination coverage can substantially reduce coinfection cases. .

In Figure 4.7, there are four different plots. For the Effect of COVID-19 Vaccine Failure

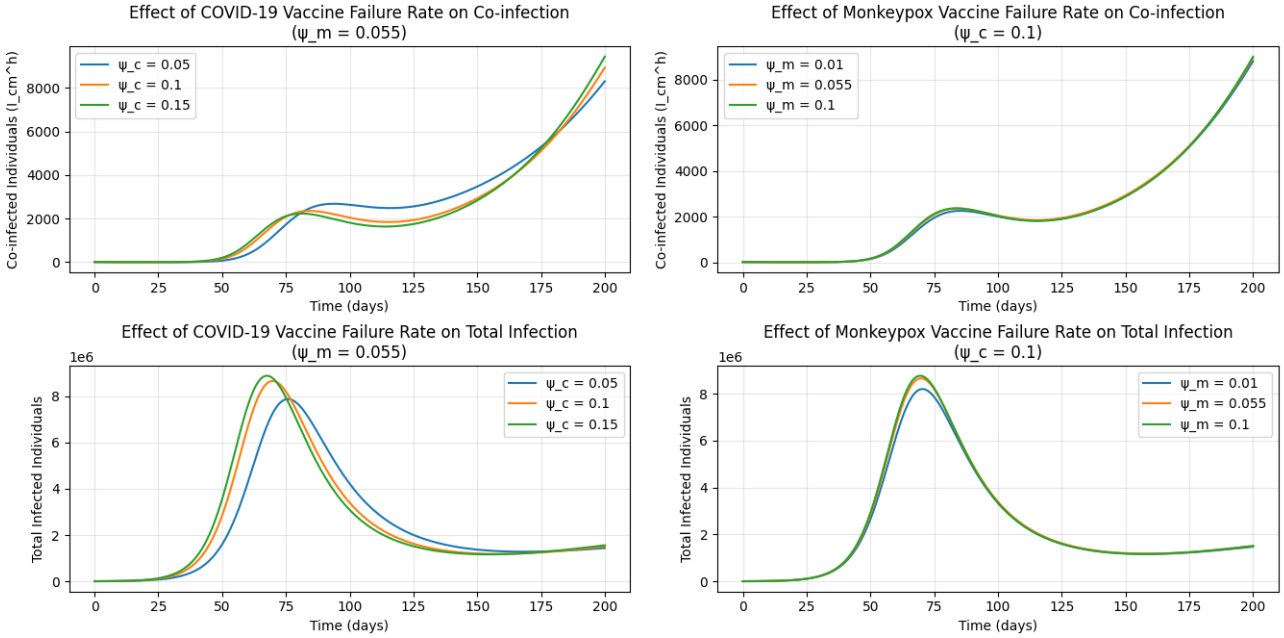

Figure 5: Effect of Vaccination Failure on Coinfection and Total Infection

(ψ_c) on Co-infection, the plot illustrates that as the COVID-19 vaccine failure rate (ψ_c) increases from 0.05 to 0.15, the number of co-infected individuals ($I_c^h m$) significantly rises. A higher ψ_c corresponds to a higher line on the graph. Increased vaccine failure (ψ_c) results in more vaccinated individuals (V_c) becoming susceptible again and contracting the virus, thus expanding the pool of individuals infected with COVID-19 (I_c^h). A larger I_c^h pool increases the chances of also contracting monkeypox (via the $\pi\lambda_m I_c^h$ term in the $\frac{dI_c^h m}{dt}$ equation), contributing to a rise in co-infections.

For the Effect of Monkeypox Vaccine Failure (ψ_m) on Co-infection, a similar trend is observed. As the Monkeypox vaccine failure rate (ψ_m) increases from 0.01 to 0.1, the number of co-infected individuals also rises. Lower efficacy of the monkeypox vaccine leads to a greater susceptibility to monkeypox, resulting in a larger I_m^h pool. This increased pool of monkeypox-infected individuals is more likely to contract COVID-19 (via the $\pi\lambda_c I_m^h$ term), further increasing the co-infection count.

For the Effect of COVID-19 Vaccine Failure (ψ_c) on Total Infection, the plot displays the total number of individuals infected with both diseases ($I_c^h + I_m^h + I_{cm}^h$). Higher ψ_c values considerably elevate the overall disease burden in the population, illustrating the interconnected nature of the problems caused by a failing COVID-19 vaccine; this does not only heighten COVID-19 cases but also facilitates more monkeypox cases and increases co-

infections. A failure to control one pathogen negatively impacts public health outcomes.

Lastly, for the Effect of Monkeypox Vaccine Failure (ψ_m) on Total Infection, the same pattern is evident; higher ψ_m results in a greater total number of infected individuals. The failure of the monkeypox vaccine similarly undermines control efforts for both diseases and amplifies overall infection prevalence. The plots provide quantitative evidence that the efficacy of both vaccines is critical for managing not only each specific disease but also the co-epidemic situation as a whole. This indicates a synergistic negative effect, where the failure of one vaccine intensifies the spread of the other disease and exacerbates the problem of co-infections. The model demonstrates that vaccination programs are not solely about individual protection; they serve a collective benefit by reducing the pathogen reservoir in a community. High-efficacy vaccines (low ψ) act as a robust barrier, slowing or halting transmission. It is essential for public health agencies to emphasize the deployment of high-efficacy vaccines. The model suggests that selecting a vaccine with 85% efficacy ($\psi = 0.15$) instead of one with 95% efficacy ($\psi = 0.05$) could result in significantly poorer outbreak outcomes, particularly in scenarios where both diseases circulate simultaneously.

The parameter ω (waning immunity) functions similarly to ψ (vaccine failure) within the model by transitioning individuals from the recovered class (R_h) back to the susceptible class (S_h). This model points out that in a co-epidemic context, waning immunity presents a substantial challenge, continually introducing new susceptible individuals into the population and exacerbating both outbreaks. This highlights the importance of booster shots for maintaining population immunity, especially in high-risk settings. Moreover, this model transcends the notion of single-disease analysis. It shows that in environments where multiple pathogens coexist, the success of interventions against one disease affects vulnerability to others. High-efficacy vaccination is essential; it is not an option but a crucial strategy for averting complex health crises that arise from synergistic outbreaks. The 'firewalls' established against one disease also contribute to protection against others.

Figure 4.8 illustrates both 2D and 3D contour plots that visualize the effects of varying quarantine rates for COVID-19 and monkeypox on the peak infections of each disease and their co-infection. The COVID-19 quarantine rate (ζ_c) ranges from 0.05 to 0.1 per day, while the monkeypox quarantine rate (ζ_m) varies from 0.02 to 0.05 per day. The 2D contour plots enable clear visualization of the relationship between quarantine rates and infection peaks, whereas the 3D contour plots provide a more comprehensive view. Different colormaps are used for each disease to enhance visual distinction, and color intensity signifies the magnitude of peak infections. The COVID-19 plot demonstrates decreasing infection peaks with higher COVID-19 quarantine rates, with minimal impact from monkeypox quarantine. Conversely, the monkeypox plot indicates decreasing infection peaks with increased monkeypox quarantine rates, with COVID-19 quarantine having minimal effect. The co-infection plot shows decreasing trends with rises in either quarantine rate, indicating that quarantine measures against either disease can lower co-infection rates. The contour lines represent levels of equal infection prevalence, aiding public health officials in identifying the necessary combination of quarantine rates to achieve specific infection control targets. The steepness of the contours indicates the sensitivity of each disease to changes in quarantine measures. The steep gradients along the (ζ_c) axis suggest that COVID-19-specific quarantine measures significantly decrease COVID-19 transmission, reflecting the effectiveness of early case identification and isolation for respiratory viruses.

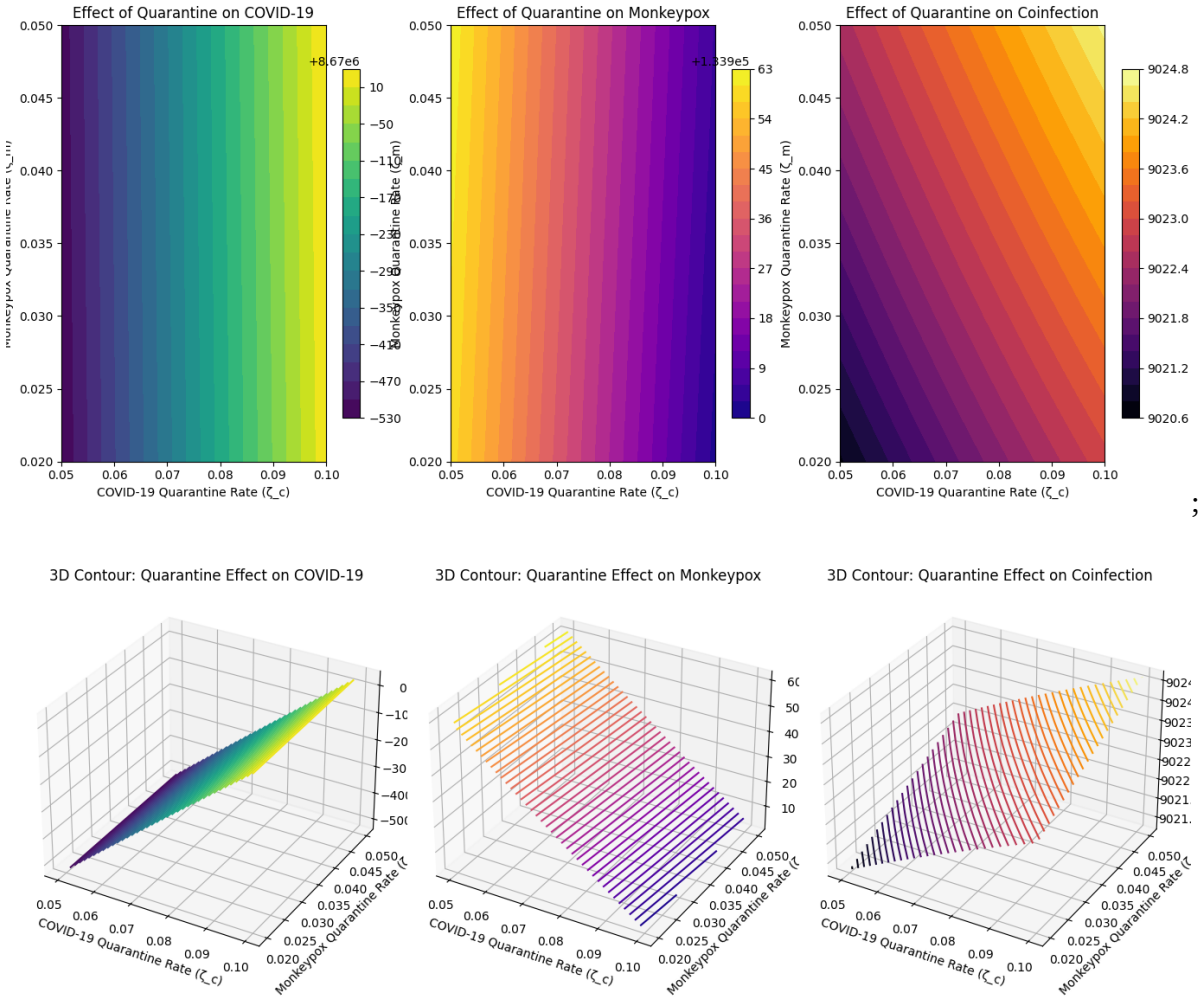

Figure 6: Effect of Quarantine on COVID-19, Monkeypox and Coinfection

In contrast, the less steep gradients imply that monkeypox quarantine is somewhat less effective, possibly due to a longer incubation period, challenges in early detection, and symptom-based limitations. The contour patterns indicate that simultaneous quarantine of both diseases offers heightened protection against co-infection, exceeding the sum of the individual effects. The basic reproduction number (R_0) for COVID-19 is generally higher than that of monkeypox, making containment measures more impactful. Overall, these biological interpretations underline that while quarantine is an effective tool for controlling both individual diseases and their co-infection, the effectiveness varies significantly due to differing biological characteristics. The optimal quarantine strategy should balance disease-specific approaches with integrated surveillance systems capable of detecting both infections simultaneously. The contour patterns provide a quantitative framework for public health decision-making, illustrating how different distributions of quarantine resources influence disease outcomes and emphasizing the important role of quarantine in preventing challenging co-infection cases.

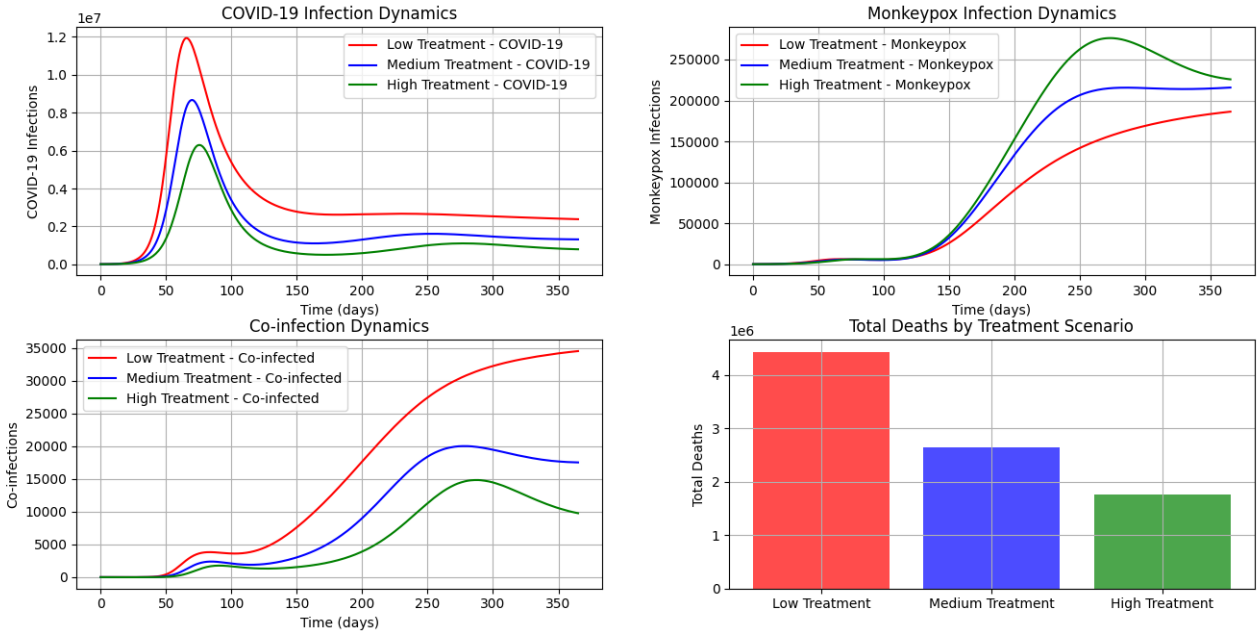

Figure 7: Effect of Treatment Rate on COVID-19, Monkeypox and Coinfection

In figure 4.9, there are three different plots, including one for the Treatment Scenario. For the COVID-19 Infection Dynamics plot, the Low Treatment scenario (red) results in the highest peak of COVID-19 infections. As treatment rates increase to Medium (blue) and High (green), the peak number of active infections decreases significantly. This outcome arises because infected individuals are treated and removed from the infectious pool (I_c^h) more quickly, which in turn slows transmission. The Outbreak Duration shows that the Low Treatment curve is wider and flatter after the peak, indicating a longer "tail" of the outbreak, during which the disease circulates at a lower level for an extended period. Conversely, the High Treatment scenario demonstrates a sharper decline after the peak, suggesting that the outbreak is controlled more swiftly. This graph indicates that effective

COVID-19 treatment is important not only for reducing the overall number of cases (the area under the curve) and preventing healthcare system overload (lower peak) but also for shortening the duration of the outbreak.

For the Monkeypox Infection Dynamics plot, similar to the COVID-19 plot, stronger treatment leads to a lower peak of monkeypox infections. However, the effect may be slightly less pronounced than for COVID-19, based on the selected parameter values. This is attributed to the influence of the rodent reservoir $(\mathrm{I_r})$, which is not directly affected by human treatment rates. Despite the treatment parameter γ_{m} specifically targeting monkeypox, an increase in COVID-19 treatment also has a positive effect (compare the red "Low" line to the blue/green lines). This finding highlights an important aspect of co-infection dynamics: successfully treating COVID-19 reduces the number of individuals who are severely ill and susceptible to co-infection, thereby indirectly mitigating the monkeypox outbreak by decreasing the pool of potential co-infected hosts.

For the Co-infection Dynamics plot, the impact of treatment is most pronounced. The Low Treatment scenario leads to a significant wave of co-infections, while the High Treatment scenario suppresses this wave almost entirely. This suggests that an integrated treatment strategy is essential. Focusing on simultaneous treatment of both diseases is the most effective way to prevent serious medical complications and high mortality rates associated with co-infection. Finally, the Total Deaths by Treatment Scenario bar chart exhibits a steep, monotonic decrease in total deaths as treatment intensity rises from Low to Medium to High. The reduction in deaths directly correlates with the trends observed in the other three plots, quantifying the ultimate human cost. It demonstrates that investing in comprehensive treatment capacity for both diseases saves lives, and the benefits from this investment (in terms of lives saved) are significant. Overall, increasing treatment rates for COVID-19 (γ_{c}), monkeypox (γ_{m}), and co-infection (γ_{cm}) results in improved outcomes across various measures: lower infection peaks, shorter outbreak durations, and significantly fewer deaths. The substantial reduction in co-infections under the High Treatment scenario indicates that co-infection is not an unavoidable consequence of simultaneous outbreaks, but rather a preventable outcome that can be managed through effective public health interventions focused on both diseases.

4. Conclusion

In this research, a complete analysis of a COVID-19 and Monkeypox co-infection disease model using optimal control theory has been carried out to extend the existing theoretical findings of the initial research work [16]. The study established the mathematical well-posedness and biological feasibility of the model, demonstrating its capability to describe the transmission dynamics of both diseases under realistic epidemiological conditions.

Sensitivity analysis provided quantitative insights into the parameters that most strongly influence disease transmission. The results showed that transmission and progression rates have the greatest impact on the reproduction numbers, while quarantine, treatment, and vaccination play critical roles in reducing disease spread. These findings emphasize the importance of strengthening public health interventions focused on effective quarantine, timely treatment, and sustained vaccination programs.

Furthermore, the optimal control analysis revealed that cost-effective management of COVID-19–Monkeypox co-infection requires a combined strategy involving vaccination, quarantine, and treatment. The implementation of time-dependent controls significantly reduced both single infections and coinfection cases, highlighting the benefits of adaptive intervention strategies.

In conclusion, this work contributes to the growing literature on infectious disease co-infection modeling by providing a comprehensive mathematical framework and optimal control strategy for COVID-19 and Monkeypox transmission dynamics. The findings offer valuable insights for policymakers and public health authorities in designing effective intervention measures during concurrent outbreaks. Future research may extend this model by incorporating stochastic effects, spatial heterogeneity, age structure, and real-time data fitting. In addition, the development of a fractional-order COVID-19–Monkeypox co-infection model is recommended, as fractional derivatives can capture memory and hereditary effects in disease transmission processes. Such an extension may provide a more realistic representation of epidemic dynamics and improve the prediction and control of co-infection outbreaks.

Acknowledgement

We would like to sincerely acknowledge the insightful guidance, constructive criticisms, and motivating suggestions given by our peers and reviewers while preparing this paper. These have been instrumental in improving the standard of this paper.

References

[1] World Health Organization (WHO), 2020. *Coronavirus disease (COVID-19) pandemic*. Situation Reports, WHO, Geneva.

[2] World Health Organization (WHO), 2022. *Multi-country outbreak of monkeypox*. Situation Reports, WHO, Geneva.

[3] Anderson, R. M., Vegvari, C., Truscott, J., and Collyer, B. S., 2021. Challenges in creating herd immunity to SARS-CoV-2. *Vaccine*, 39(16), 2453–2462.

[4] Eze, F. C., and Uwaezuoke, M. U. (2025).Age-structured deterministic model for the dynamics of Hepatitis B virus in Nigeria incorporating vertical and horizontal transmission.*International Journal of Mathematical and Applied Modelling*, 8 (2), 212-251.

[5] Omame, A., Raezah, A.A., Okeke, G.A. et al. Assessing the impact of intervention measures in a mathematical model for monkeypox and COVID-19 co-dynamics in a high-risk population. Model. Earth Syst. Environ. 10, 6341–6355 (2024). https://doi.org/10.1007/s40808-024-02132-x
[6] Bunge, E. M., Hoet, B., Chen, L., Lienert, F., Weidenthaler, H., Baer, L., and Steffen, R., 2022. The changing epidemiology of human monkeypox—A potential threat? *PLOS Neglected Tropical Diseases*, 16(2), e0010141.
[7] Cox, M. J., Loman, N., Bogaert, D., and O'Grady, J., 2020. Co-infections: Potentially lethal and unexplored in COVID-19. *The Lancet Microbe*, 1(1), e11.
[8] Al-Tawfiq, J. A., Barry, K., and Memish, Z. A., 2022. Emerging viral infections: Coinfection dynamics and implications. *Travel Medicine and Infectious Disease*, 49, 102384.
[9] Kermack, W. O., and McKendrick, A. G., 1927.A contribution to the mathematical theory of epidemics. *Proceedings of the Royal Society A*, 115, 700–721.
[10] Eze, F. C., Idowu, K. O., Adam, U. M., and Olofin, D. O. (2025).Mathematical modelling of the endemic phase of COVID-19 infection considering vaccination breakthrough, revaccination and reinfection.*International Journal of Applied Mathematics and Modelling*, 8(2), 148-180.
[11] Hethcote, H. W., 2000. The mathematics of infectious diseases. *SIAM Review*, 42(4), 599–653.
[12] Ivorra, B., Ferrández, M. R., Vela-Pérez, M., and Ramos, A. M., 2020. Mathematical modeling of the spread of the coronavirus disease 2019 (COVID-19). *Mathematical Modelling of Natural Phenomena*, 15, 33.
[13] Okuonghae, D., and Omame, A., 2020. Analysis of a mathematical model for COVID-19 population dynamics in Nigeria. *Chaos, Solitons & Fractals*, 139, 110032.
[14] Grant, R., Nguyen, L., and Breen, R., 2020. Modelling human-to-human transmission of monkeypox. *Epidemics*, 31, 100401.
[15] Peter, O. J., Ogunseye, S. A., Oguntolu, S. A., and Ibrahim, O. A., 2022. Mathematical model for monkeypox transmission dynamics. *Data in Brief*, 42, 108190.
[16] Eze, F. C., Obi, M. C., Iheonu, N. O., and Araka, N. N., & Godwin, E. C 2026. A mathematical model for the dynamics of COVID-19 and Monkeypox co-infection considering the effects of vaccination, quarantine, and reinfection. *Journal of Mathematical Analysis and Modeling*, vol 7 (1). https://doi.org/10.48185/jmam.v7i1.1915
[17] Chitnis, N., Hyman, J. M., and Cushing, J. M., 2008. Determining important parameters in the spread of malaria through the sensitivity analysis of a mathematical model. *Bulletin of Mathematical Biology*, 70(5), 1272–1296.
[18] Marino, S., Hogue, I. B., Ray, C. J., and Kirschner, D. E., 2008. A methodology for performing global uncertainty and sensitivity analysis in systems biology. *Journal of Theoretical Biology*, 254(1), 178–196.
[19] Jung, E., Lenhart, S., and Feng, Z., 2005. Optimal control of treatments in a two-strain tuberculosis model.*Mathematical Biosciences and Engineering*, 2(3), 473–482.
[20] Eze, F. C., Iwa, L. L., Adam, U. M., and Audu, A. M. (2025).A mathematical analysis of tuberculosis transmission using a two-age group compartmental model.*Journal of Mathematical Analysis and Modeling*, 6(2), 100–126. https://doi.org/10.48185/jmam.v6i2.1657
[21] Lenhart, S., and Workman, J. T., 2007. *Optimal Control Applied to Biological Models*. Chapman & Hall/CRC, Boca Raton, FL.
[22] Florida Department of Health (2022). Florida Population Estimates.
[23] Florida Department of Health (2022). COVID-19 Vaccination Report.
[24] Florida Department of Health (2022). COVID-19 Dashboard.
[25] Florida Department of Health (2022). Monkeypox Outbreak Data.
[26] Obi, V. O., Eze, F., and Nwajeri, K. U. (2025).Transmission dynamics of cholera disease using fractional-order model.*Journal of Mathematical Analysis and Modeling*, 6(3), 84–112.
[27] Centers for Disease Control and Prevention (CDC) (2022). Monkeypox in Animals.
[28] CDC (2022). Monkeypox Vaccine Administration.
[29] CDC (2020). COVID-19 Control Guidelines.
[30] World Health Organization (WHO) (2022). COVID-19 Dashboard.
[31] Eze, F. C., Nwadibia, A. I., Inyama, S. C., Omame, A., and Godwin, E. C. (2020).Analysis of the transmission dynamics for Zika virus with nonlinear force of infections.*Journal of Mathematical Sciences & Computational Mathematics*, 1(2), 119–165. https://doi.org/10.15864/jmscm.1201
[32] WHO (2022). Monkeypox Multi-country Outbreak Report.
[33] WHO (2022). Monkeypox Control Guidelines.

[34] Patel, A., Bilinska, J., Tam, J. C. H., et al. (2022). Clinical features and management of human monkeypox.
[35] United States Census Bureau (2022). Population Data.
[36] Davis, S., & Calvet, E. (2002). Rodent population dynamics and disease transmission.
[37] Zhang, J., Litvinova, M., Liang, Y., et al. (2020).Changes in contact patterns shape COVID-19 dynamics.
[38] Nwadibia, A. I., Eze, F. C., Inyama, S. C., Nse, C. A., Omame, A., and Mbachu, H. I. (2018).Mathematical model of the transmission dynamics of genital elephantiasis (lymphatic filariasis).*Mathematical Theory and Modeling*, 8(4), 71–113.
[39] UK Health Security Agency (2022). Epidemiology of Monkeypox in England.
[40] UKHSA (2022). Monkeypox Outbreak in England.
[41] Adalja, A., & Inglesby, T. (2022). A novel coronavirus and pandemic preparedness.
[42] Lauer, S. A., Grantz, K. H., Bi, Q., et al. (2020). Incubation period of COVID-19.
[43] Mathieu, E., Ritchie, H., Rodés-Guirao, L., et al. (2024). COVID-19 vaccination data.
[44] Thompson, M. G., Burgess, J. L., Naleway, A. L., et al. (2021).Effectiveness of COVID-19 vaccines.
[45] Stokes, E. K., Zambrano, L. D., Anderson, K. N., et al. (2020). Coronavirus disease case surveillance.
[46] Arias, E., & Xu, J. (2021). United States Life Tables.
[47] Goldberg, Y., Mandel, M., Bar-On, Y. M., et al. (2021). Waning immunity after COVID-19 vaccination.
[48] Jeelani, M. B., Alnahdi, A. S., Abdo, M. S., Abdulwasaa, M. A., Shah, K., & Wahash, H. A. (2021). Mathematical modeling and forecasting of COVID-19 in Saudi Arabia under fractal-fractional derivative in Caputo sense with power-law. *Axioms*, **10**(3), 228. https://doi.org/10.3390/axioms10030228
[49] Thabet, S. T. M., Abdo, M. S., & Shah, K. (2021). Theoretical and numerical analysis for transmission dynamics of COVID-19 mathematical model involving Caputo–Fabrizio derivative. *Advances in Difference Equations*, **2021**(1), 184. https://doi.org/10.1186/s13662-021-03316-w